

Letter

Size effects in the interface level alignment of dye-sensitized TiO₂ clusters

Noa Marom, Thomas Körzdörfer, Xinguo Ren, Alexandre Tkatchenko, and James R. Chelikowsky

J. Phys. Chem. Lett., **Just Accepted Manuscript** • Publication Date (Web): 19 Jun 2014

Downloaded from <http://pubs.acs.org> on June 24, 2014

Just Accepted

“Just Accepted” manuscripts have been peer-reviewed and accepted for publication. They are posted online prior to technical editing, formatting for publication and author proofing. The American Chemical Society provides “Just Accepted” as a free service to the research community to expedite the dissemination of scientific material as soon as possible after acceptance. “Just Accepted” manuscripts appear in full in PDF format accompanied by an HTML abstract. “Just Accepted” manuscripts have been fully peer reviewed, but should not be considered the official version of record. They are accessible to all readers and citable by the Digital Object Identifier (DOI®). “Just Accepted” is an optional service offered to authors. Therefore, the “Just Accepted” Web site may not include all articles that will be published in the journal. After a manuscript is technically edited and formatted, it will be removed from the “Just Accepted” Web site and published as an ASAP article. Note that technical editing may introduce minor changes to the manuscript text and/or graphics which could affect content, and all legal disclaimers and ethical guidelines that apply to the journal pertain. ACS cannot be held responsible for errors or consequences arising from the use of information contained in these “Just Accepted” manuscripts.

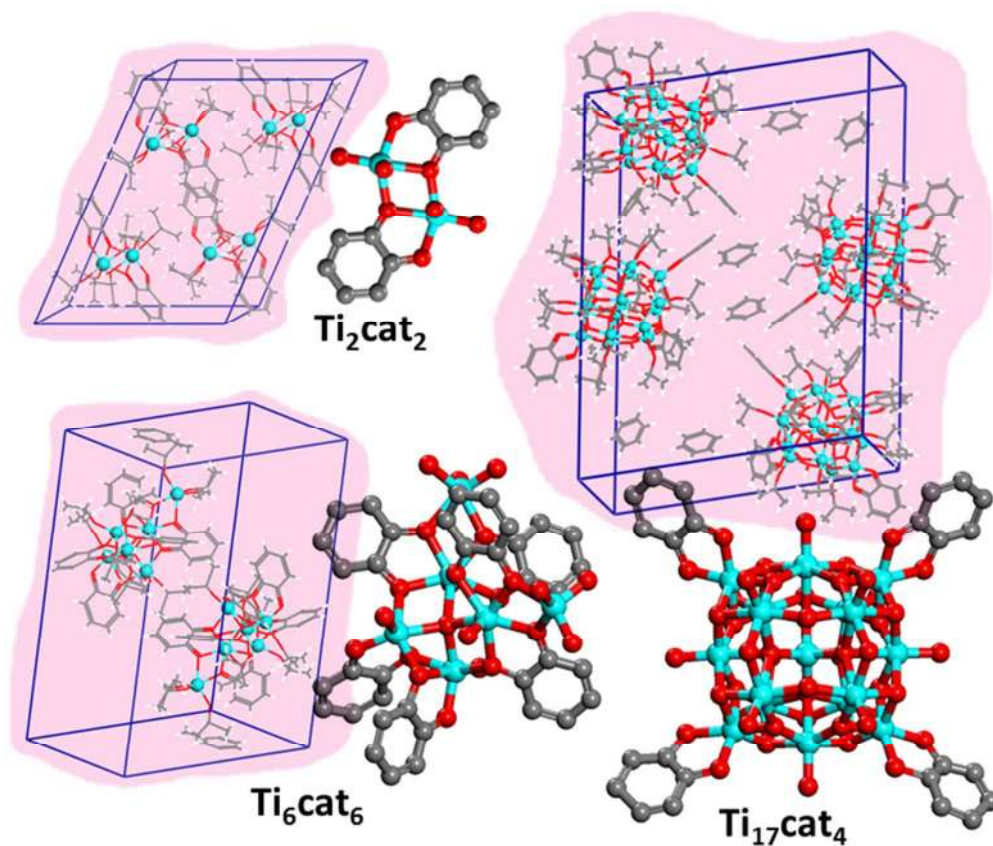


Figure 1. Illustrations of the unit cells of the crystalline phases of TiO₂ clusters sensitized with catechol from Ref. 7 and of the reduced structures without the isopropoxy (IPr) moieties (hydrogen atoms are not shown for clarity). Ti₂cat₂, Ti₆cat₆, and Ti₁₇cat₄ comprise TiO₂ clusters with 2, 6, and 17 Ti atoms, functionalized with 2, 6, and 4 catechol (cat) molecules, respectively. Ti atoms are colored in cyan, O atoms in red, C atoms in gray, and H atoms in white.
200x169mm (96 x 96 DPI)

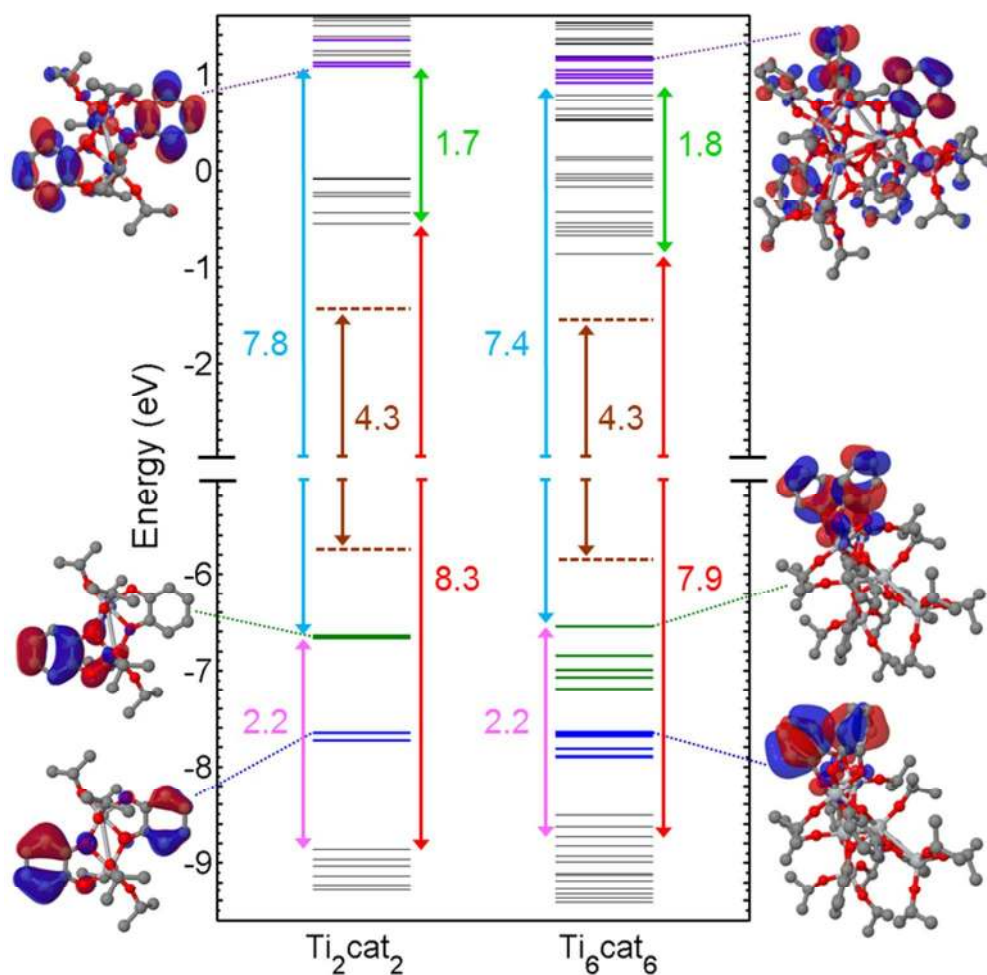


Figure 3. The interface level alignment of Ti_2cat_2 and Ti_6cat_6 . Red arrows indicate the cluster gap, light blue arrows indicate the catechol gap, pink arrows indicate the alignment between the catechol HOMO and the cluster's valence states, light green arrows indicate the alignment between the catechol LUMO and the cluster's empty states, brown dashed lines indicate the narrowing of the gap due to polarization, brown arrows indicate the gap of the crystalline phases of Ti_2cat_2 and Ti_6cat_6 , estimated from the polarization model. Illustrations of Ti_2cat_2 and Ti_6cat_6 orbitals associated with the LUMO, HOMO, and HOMO-1 of catechol are also shown.

229x224mm (96 x 96 DPI)

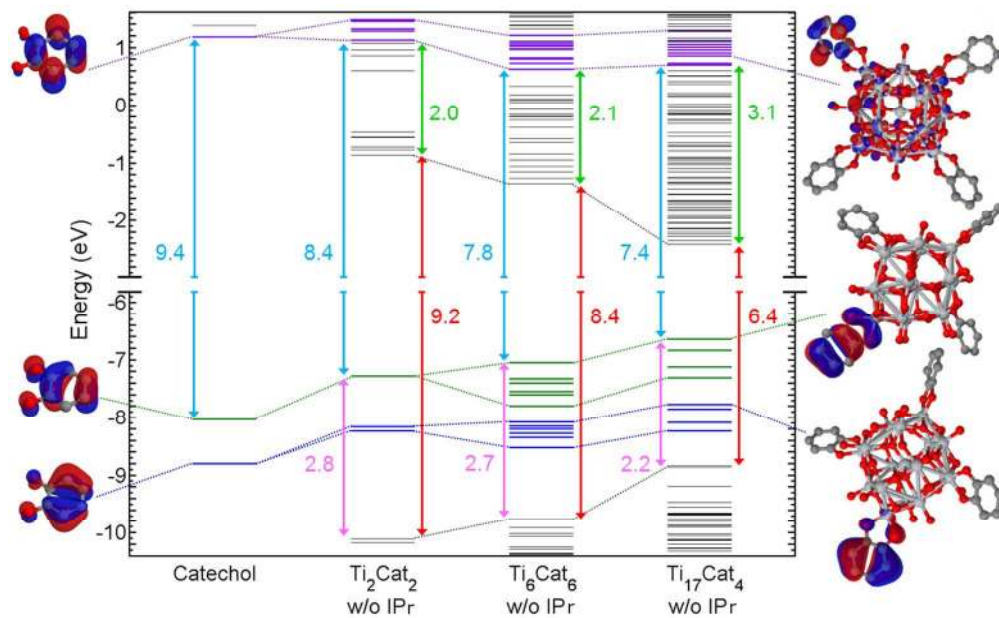


Figure 2. Size effects in the interface level alignment between catechol and increasingly large TiO₂ clusters. Red arrows indicate the cluster gap, light blue arrows indicate the catechol gap, pink arrows indicate the alignment between the catechol HOMO and the cluster's valence states, light green arrows indicate the alignment between the catechol LUMO and the cluster's empty states. Illustrations of the frontier orbitals of catechol in the gas phase and attached to the largest cluster are also shown.

355x219mm (96 x 96 DPI)

Size Effects in the Interface Level Alignment of Dye-Sensitized TiO₂ clusters

Noa Marom,^{*,1,2} Thomas Körzdörfer,³ Xinguo Ren,⁴ Alexandre Tkatchenko,⁵ and James R. Chelikowsky²

¹Physics and Engineering Physics, Tulane University, New Orleans, Louisiana 70118, USA

²Institute for Computational Engineering and Sciences (ICES), The University of Texas at Austin, Austin, Texas 78712, USA

³Computational Chemistry, University of Potsdam, 14476 Potsdam, Germany

⁴Key Laboratory of Quantum Information, University of Science and Technology of China, Hefei, Anhui, 230026, China

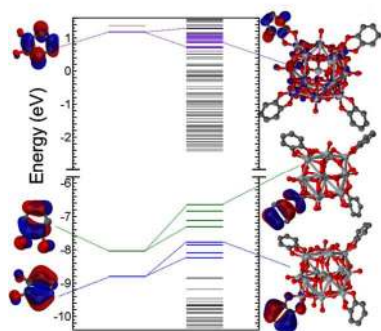
⁵Fritz-Haber-Institut der Max-Planck-Gesellschaft, Faradayweg 4-6, 14195, Berlin, Germany

ABSTRACT

The efficiency of dye-sensitized solar cells (DSCs) depends critically on the electronic structure of the interfaces in the active region. We employ recently developed dispersion-inclusive density functional theory (DFT) and GW methods to study the electronic structure of TiO₂ clusters sensitized with catechol molecules. We show that the energy level alignment at the

dye-TiO₂ interface is the result of an intricate interplay of quantum size effects and dynamic screening effects and that it may be manipulated by nano-structuring and functionalizing the TiO₂. We demonstrate that the energy difference between the catechol LUMO and the TiO₂ LUMO, which is associated with the injection loss in DSCs, may be reduced significantly by reducing the dimensions of nano-structured TiO₂ and by functionalizing the TiO₂ with wide-gap moieties, which contribute additional screening but do not interact strongly with the frontier orbitals of the TiO₂ and the dye. Precise control of the electronic structure may be achieved via “interface engineering” in functional nanostructures.

TOC



KEYWORDS Dye-sensitized solar cell, interface engineering, functional nanostructure, quantum size effect, electronic structure, DFT, GW approximation, dispersion interactions, many-body dispersion, van der Waals

1
2
3 Nobel laureate Herbert Kroemer coined the phrase “the interface is the device”.¹ This is certainly
4 true for dye-sensitized solar cells (DSCs).²⁻⁵ DSCs are hybrid organic-inorganic systems. As
5 such, they enjoy the best of both worlds by combining the high charge carrier mobility and
6 efficient electrical charge injection of the inorganic component with the strong light-matter
7 coupling and rich chemical compound space of the organic component. In DSCs sunlight is
8 harvested by (metal-) organic dyes, attached to a nano-structured oxide, typically TiO₂. Charge
9 separation is achieved at the dye-oxide interface via electron injection from the lowest
10 unoccupied molecular orbital (LUMO) of the dye into the conduction band of the oxide.
11 Regeneration occurs via hole transfer from the highest occupied molecular orbital (HOMO) of
12 the dye to a hole conductor (often, a redox pair in solution). The energy differences between the
13 dye LUMO (HOMO) and the oxide conduction band edge (redox potential) provide the driving
14 force for injection (regeneration). These unavoidable injection and regeneration losses reduce the
15 maximal open circuit voltage of a DSC. Typically, an energy difference of a fraction of an eV at
16 the interface is considered to provide a good balance between the injection (regeneration)
17 efficiency and the voltage loss.³ Thus, the efficiency of a DSC depends critically on the
18 electronic structure of the interfaces in its active region.

19
20
21
22
23
24
25
26
27
28
29
30
31
32
33
34
35
36
37
38
39
40
41 Owing to quantum effects at the nano-scale, the energy level alignment at the interface
42 depends strongly on the local environment and cannot be derived directly from the positions of
43 the energy levels of isolated species. First, the gap of a molecule on a surface narrows with
44 respect to its gas phase gap because of screening.⁶⁻¹⁴ Second, the electronic properties of nano-
45 structured TiO₂ depend strongly on size and structure.¹⁵⁻¹⁸ Third, the orientation of dye
46 molecules with respect to the oxide surface affects the coupling at the interface and may alter the
47 conditions for charge transfer.¹⁹⁻²² Interfaces in DSCs are typically disordered and their measured
48
49
50
51
52
53
54
55
56
57
58
59
60

1
2
3 properties, such as the open circuit voltage, must be regarded as an average over several
4 configurations, some of which are better than others. In addition to harboring some less than
5 optimal configurations, disorder may cause losses due to traps and tail states.²³ The incomplete
6 understanding of all the factors affecting the electronic structure and functionality of these
7 interfaces and the lack of clear design rules have led to the perception that disorder is essential,
8 rather than detrimental, to the operation of DSCs because it is on average better than a less than
9 optimal order.
10
11
12
13
14
15
16
17
18

19
20 First principles quantum mechanical simulations enable a systematic investigation of nano-
21 structured interfaces to elucidate the relations between structural configuration and electronic
22 properties and to derive design rules for more efficient DSCs. The present study focuses on how
23 the energy level alignment at the dye-TiO₂ interface may be manipulated by nano-structuring and
24 functionalizing the TiO₂. It is demonstrated that the interface level alignment is the result of an
25 intricate interplay of quantum size effects and dynamic screening effects. The energy difference
26 between the catechol LUMO and the TiO₂ LUMO, which is associated with the injection loss,
27 may be reduced significantly by reducing the dimensions of nano-structured TiO₂ and by
28 functionalizing the TiO₂ with wide-gap moieties, which contribute additional screening but do
29 not interact strongly with the frontier orbitals of the TiO₂ and the dye. Precise control of the
30 electronic structure may be achieved via “interface engineering”.
31
32
33
34
35
36
37
38
39
40
41
42
43
44
45

46 We examine three of the crystalline nano-cluster phases synthesized by Benedict and
47 Coppens,²⁴ shown in Fig. 1. They comprise TiO₂ clusters of increasing size, functionalized with
48 catechol (cat) molecules, and terminated with isopropoxy (IPr) moieties, such that the Ti atoms
49 are 6-coordinated. Ti₂cat₂, Ti₆cat₆, and Ti₁₇cat₄ comprise 2, 6, and 17 Ti atoms and 2, 6, and 4
50 catechol molecules, respectively. These systems are useful models for fundamental studies of the
51
52
53
54
55
56
57
58
59
60

dye-TiO₂ interface because they have a well-defined structure, characterized by single crystal x-ray diffraction (XRD). In Ref. 25 the interface level alignment of Ti₂cat₂ was compared to that of a system comprising a TiO₂ cluster of a similar size functionalized with isonicotinic acid (INA). Here, it is compared to systems comprising larger TiO₂ clusters to elucidate size effects. The catechol molecule and the TiO₂ clusters studied here are much smaller than the dyes and TiO₂ particles typically used in DSCs, which makes them amenable to high accuracy *ab initio* simulations.

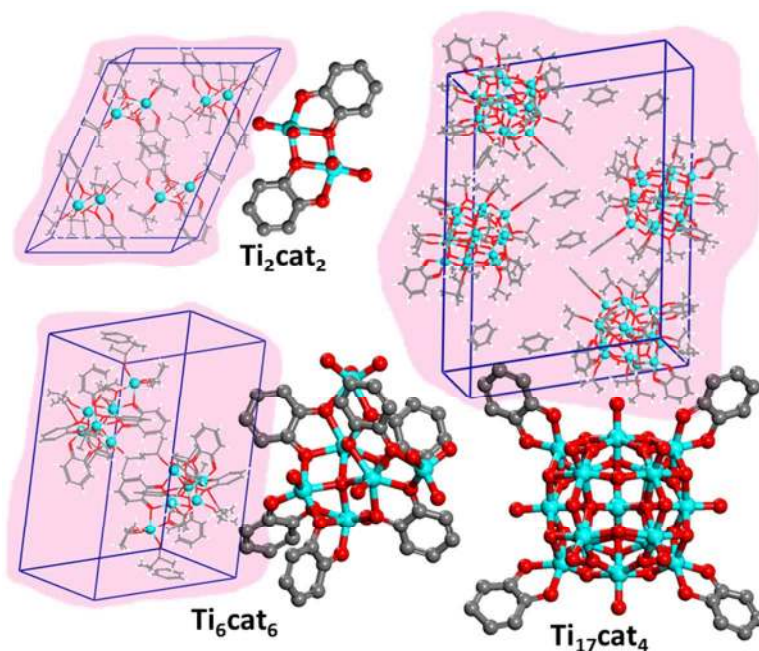


Figure 1. Illustrations of the unit cells of the crystalline phases of TiO₂ clusters sensitized with catechol from Ref. 7 and of the reduced structures without the isopropoxy (IPr) moieties (hydrogen atoms are not shown for clarity). Ti₂cat₂, Ti₆cat₆, and Ti₁₇cat₄ comprise TiO₂ clusters with 2, 6, and 17 Ti atoms, functionalized with 2, 6, and 4 catechol (cat) molecules, respectively. Ti atoms are colored in cyan, O atoms in red, C atoms in gray, and H atoms in white.

All calculations were performed with the all-electron numerical atom-centered orbital (NAO) code, FHI-aims²⁶⁻²⁸ using *tier 2* basis sets. In Ref 25, the internal parameters of the Ti₂cat₂ unit cell (376 atoms) were relaxed using dispersion-inclusive density functional theory (DFT) with

1
2
3 the Perdew-Burke-Ernzerhof (PBE)²⁹⁻³⁰ exchange-correlation functional and the Tkatchenko-
4 Scheffler (TS)³¹ dispersion method. It was shown that the atomic positions obtained with
5 PBE+TS overlapped the XRD structure almost exactly. Here, owing to the size of the Ti₆cat₆,
6 and Ti₁₇cat₄ unit cells (408 and 1172 atoms, respectively) only the hydrogen positions were
7 relaxed because these are determined less accurately from XRD. In particular, for Ti₁₇cat₄
8 hydrogen positions were not reported in Ref. 24. The structure of the unit cell with relaxed
9 hydrogen positions is provided in the supporting information. We note that H atoms were also
10 added on four bridging oxygen sites, which otherwise produce gap states.
11
12
13
14
15
16
17
18
19
20
21

22 An accurate description of the fundamental gaps and the level alignment at interfaces calls for
23 a treatment beyond ground state DFT. Here, we employ many-body perturbation theory within
24 the GW approximation.³²⁻³⁴ In this approximation the self-energy is obtained from the product of
25 the one-particle Green's function, *G*, and the dynamically screened Coulomb interaction, *W*.
26 Owing to the computational cost of fully self-consistent GW calculations, a perturbative
27 approach, known as *G*₀*W*₀, is typically used. The quasi-particle (QP) excitation energies are
28 obtained as a first-order correction to the DFT eigenvalues. *G* and *W* are evaluated using the
29 underlying Kohn-Sham (KS) orbitals. The *G*₀*W*₀ scheme has had some notable success in the
30 description of the electronic structure of organic-inorganic interfaces, including dye-TiO₂
31 interfaces.^{6-14, 25} In particular, *G*₀*W*₀ captures the polarization-induced renormalization of the
32 molecular energy levels at the interface, a dynamic correlation effect inherently absent from
33 standard DFT functionals.
34
35
36
37
38
39
40
41
42
43
44
45
46
47
48
49

50 To study the catechol-TiO₂ interface, non-periodic *G*₀*W*₀ calculations were performed for the
51 reduced model systems, shown in Fig. 1. The IPr moieties were removed, keeping only the
52 oxygen atoms to maintain the Ti coordination. Dangling bonds were passivated with hydrogen
53
54
55
56
57
58
59
60

1
2
3 (following the procedure of Ref. 25). The effect of functionalization with IPr was studied for
4
5 Ti_2cat_2 and Ti_6cat_6 (the $\text{Ti}_{17}\text{cat}_4$ unit, with 269 atoms, was too large for such calculations). Owing
6
7
8 to the size of some of the systems studied here, G_0W_0 calculations were performed with *tier 2*
9
10 basis sets. It has been demonstrated in Ref. 35 that at the *tier 2* level G_0W_0 spectra are already
11
12 converged in terms of the ordering and energy differences of the orbitals. The difference between
13
14 G_0W_0 spectra obtained with *tier 2* basis sets and the more converged *tier 4* basis sets typically
15
16 amounts to a rigid shift of the whole spectrum by about 0.2 eV. A comparison between the *tier 2*
17
18 and *tier 4* basis sets for the spectrum of catechol is provided as supporting information.
19
20
21

22
23 The fact that G_0W_0 QP energies are calculated non-self-consistently gives rise to a strong
24
25 dependence on the DFT starting point. This is of particular importance when semi-local DFT
26
27 functionals yield a qualitatively incorrect picture.³⁶⁻⁴² Self-interaction errors (SIE), the spurious
28
29 interaction of an electron with itself,⁴³ often render semi-local DFT inadequate as a starting point
30
31 for G_0W_0 . SIE may cause qualitative changes in the ordering of frontier molecular orbitals
32
33 because the spurious Coulomb repulsion destabilizes localized orbitals with respect to
34
35 delocalized orbitals.⁴⁴⁻⁴⁶ This effect of SIE propagates from the DFT level to the G_0W_0 level. The
36
37 inclusion of a fraction of exact exchange (EXX) in hybrid functionals mitigates SIE and provides
38
39 a better starting point for G_0W_0 calculations.^{25, 28, 35, 47-49} It has been shown that G_0W_0 based on a
40
41 good mean-field starting point may outperform GW methods at a higher level of self-
42
43 consistency, owing to error cancellation between the underscreening resulting from neglecting
44
45 the vertex and the overscreening produced by DFT functionals.³⁵ We note that in some cases, in
46
47 particular if orbital re-hybridization occurs at the interface, some form of self-consistency in the
48
49 wave-function may be required.^{13-14, 25} For the systems studied here no such re-hybridization is
50
51 found and the G_0W_0 approximation remains valid.
52
53
54
55
56
57
58
59
60

We employ a recently developed first principles method for finding a consistent starting point (CSP) for G_0W_0 .⁵⁰ This is achieved by optimizing the fraction of EXX in a global hybrid functional within the framework of generalized Kohn-Sham (GKS) theory. Using a hybrid functional starting point, the G_0W_0 QP energies, ε_i^{GoWo} , are given as follows :

$$\begin{aligned}\varepsilon_i^{GoWo} &= \varepsilon_i^{GKS} + (1 - b_{HF}) \langle \varphi_i(r) | \hat{v}_x^{HF} - v_x^{KS}[n] | \varphi_i(r) \rangle + \langle \varphi_i(r) | \hat{\Sigma}_c - v_c^{KS}[n] | \varphi_i(r) \rangle \\ &=: \varepsilon_i^{GKS} + (1 - b_{HF}) \Delta v_{x,i} + \Delta v_{c,i} \quad (1)\end{aligned}$$

where $\varphi_i(r)$ and ε_i^{KS} are the i -th DFT orbital and eigenvalue, respectively, \hat{v}_x^{HF} is the nonlocal Hartree-Fock (HF) exchange operator, $\hat{\Sigma}_c$ is the G_0W_0 correlation self-energy, $v_x^{KS}[n]$ and $v_c^{KS}[n]$ are the semi-local exchange and correlation potentials, respectively, and b_{HF} is the fraction of EXX. For orbital i , the difference between the HF and semi-local exchange energy is denoted as $\Delta v_{x,i}$ and the difference between the G_0W_0 and semi-local correlation energy is denoted as $\Delta v_{c,i}$. If a fraction of EXX can be found, such that for all orbitals:

$$(1 - b_{HF}) \Delta v_{x,i} + \Delta v_{c,i} \approx const. \quad (2)$$

then the resulting DFT eigenvalue spectrum may be considered as consistent with the G_0W_0 spectrum, in the sense that the relative orbital energies are correct and the QP correction amounts to a rigid shift of the entire spectrum. This is the essential feature of the CSP, derived in Ref.⁵⁰ The fraction of EXX in the CSP is extracted from the slope of a linear fit of $\Delta v_{c,i}$ as a function of $\Delta v_{x,i}$. Such plots for the systems studied here are provided in the supporting information. $G_0W_0@CSP$ has been shown to yield QP spectra in excellent agreement with photoemission spectroscopy (PES) experiments for various organic semiconductors.⁵⁰ The fractions of EXX in a PBE-based hybrid CSP for the systems studied here are shown in Table 1.⁵¹

Table 1. Fraction of exact exchange in the consistent starting point (CSP) used for G_0W_0 calculations of the systems studied here.

System	CSP	System	CSP
Catechol	0.28	Ti ₁₇ cat ₄ w/o IPr	0.26
Ti ₂ cat ₂ w/o IPr	0.29	Ti ₂ cat ₂	0.20
Ti ₆ cat ₆ w/o IPr	0.26	Ti ₆ cat ₆	0.19

Fig. 2 shows $G_0W_0@CSP$ energy level diagrams for Ti₂cat₂, Ti₆cat₆, and Ti₁₇cat₄ without the IPr moieties, as well as illustrations of the frontier orbitals of catechol. The orbitals associated with the HOMO, HOMO-1, and LUMO of catechol and the orbitals associated with the TiO₂ clusters may be identified by visual inspection. For all three systems the catechol HOMO and HOMO-1 lie in the gap of the TiO₂ clusters. The catechol LUMO lies in the empty state manifold of the TiO₂ clusters and is strongly hybridized with TiO₂ states. Such strong coupling between the dye LUMO and the oxide is considered favorable for electron injection. Although the three systems share some qualitative similarity, they differ in the quantitative details of the energy level alignment at the interface.

Owing to quantum size effects, the fundamental gap of the TiO₂ clusters (denoted by red arrows) narrows with increasing cluster size from 9.2 eV for the smallest cluster with 2 Ti atoms to 6.4 eV for the largest cluster with 17 Ti atoms. This is still significantly larger than the reported bulk GW gaps of 3.38-3.78 eV for rutile^{14, 52-54} and 3.79-3.83 eV for anatase^{52, 55} TiO₂.⁵⁶ This demonstrates that the band edges of TiO₂ may be tuned within a range of several eV by

nano-structuring. At the same time, the screening provided by the TiO_2 clusters also increases with size. This enhances the polarization induced gap narrowing effect, such that the gap of the catechol molecule (denoted by light blue arrows) narrows from 9.4 eV in the gas phase to 8.4 eV when attached to the smallest TiO_2 cluster and to 7.4 eV when attached to the largest TiO_2 cluster.

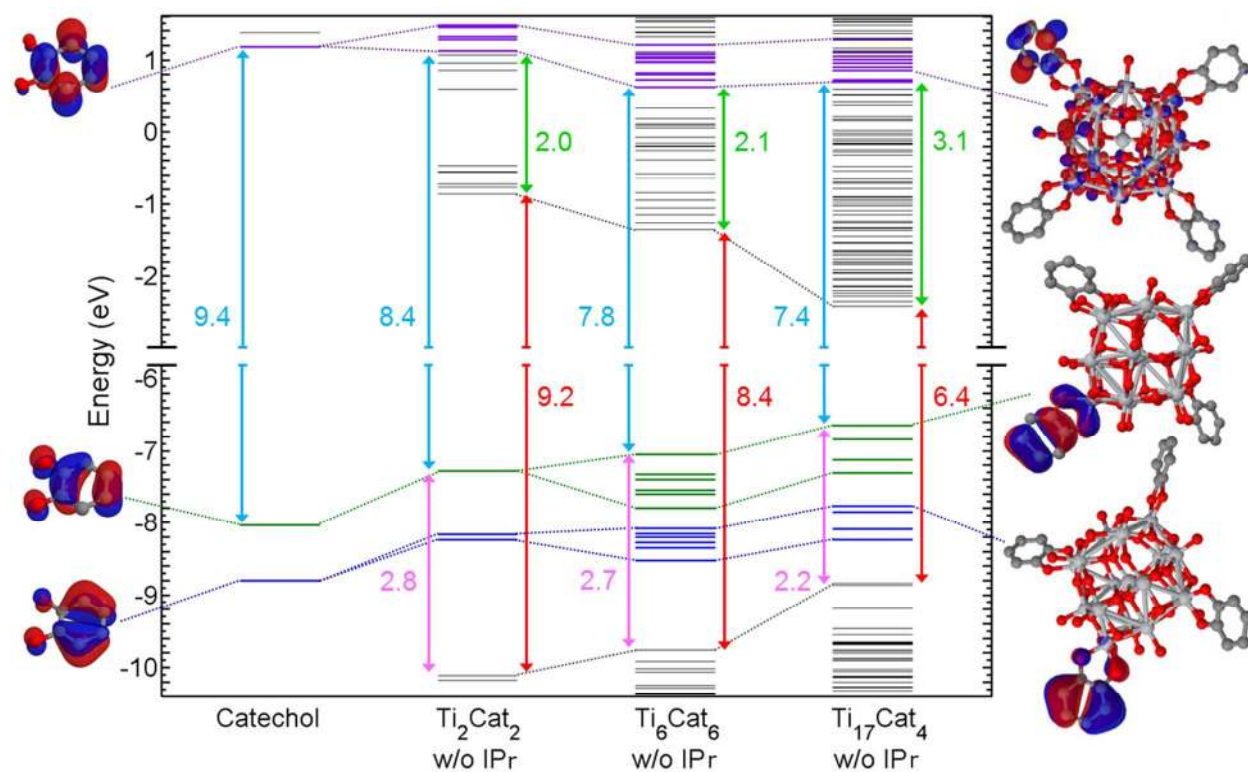


Figure 2. Size effects in the interface level alignment between catechol and increasingly large TiO_2 clusters. Red arrows indicate the cluster gap, light blue arrows indicate the catechol gap, pink arrows indicate the alignment between the catechol HOMO and the cluster's valence states, light green arrows indicate the alignment between the catechol LUMO and the cluster's empty states. Illustrations of the frontier orbitals of catechol in the gas phase and attached to the largest cluster are also shown.

The combination of quantum size effects and the polarization induced gap narrowing leads to simultaneous reduction of the gaps of the TiO_2 clusters and of the catechol molecules attached to them. The gap of the TiO_2 clusters narrows faster with system size than the gap of catechol. In addition, rather than affecting both sides of the gap equally, screening affects the position of the

catechol HOMO more strongly, while quantum confinement affects the position of the TiO₂ LUMO more strongly. As a result, the energy level alignment at the interface changes in an unintuitive way. The energy difference between the highest state associated with the catechol HOMO and the TiO₂ cluster HOMO (denoted by magenta arrows) decreases from 2.8 eV for the smallest system to 2.2 eV for the largest system. More important is the change in the energy difference between the lowest state associated with the catechol LUMO and the TiO₂ cluster LUMO (denoted by light green arrows), which grows from 2.0 eV for the smallest system to 3.1 eV for the largest system. This demonstrates that the injection loss may be reduced significantly by reducing the dimensions of nano-structured TiO₂.

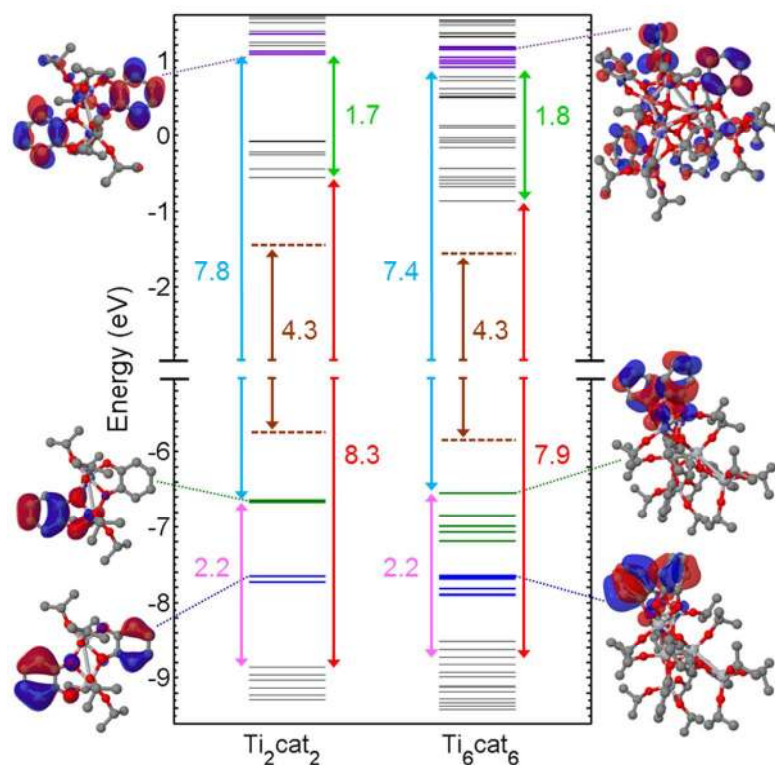


Figure 3. The interface level alignment of Ti₂cat₂ and Ti₆cat₆. Red arrows indicate the cluster gap, light blue arrows indicate the catechol gap, pink arrows indicate the alignment between the catechol HOMO and the cluster's valence states, light green arrows indicate the alignment between the catechol LUMO and the cluster's empty states, brown dashed lines indicate the narrowing of the gap due to polarization, brown arrows indicate the gap of the crystalline phases of Ti₂cat₂ and Ti₆cat₆, estimated from the polarization model. Illustrations of Ti₂cat₂ and Ti₆cat₆ orbitals associated with the LUMO,

1
2
3 Fig. 3 shows $G_0W_0@CSP$ energy level diagrams for Ti_2cat_2 and Ti_6cat_6 (with the IPr
4 moieties) and illustrations of the orbitals associated with the HOMO, HOMO-1, and LUMO of
5 catechol. As reported in Ref. ²⁵ for similar systems, the IPr moieties do not change the qualitative
6 picture of the alignment between the frontier orbitals of catechol and those of the TiO_2 clusters.
7 The HOMO of IPr hybridizes with the HOMO-2 of catechol and some valence states of the TiO_2
8 clusters. The main effect of the IPr moieties is to contribute additional screening. This leads to
9 narrowing of the TiO_2 and catechol gaps and to a decrease in the energy differences between the
10 highest orbital associated with the catechol HOMO and the TiO_2 HOMO and between the lowest
11 orbital associated with the catechol LUMO and the TiO_2 LUMO. The latter demonstrates that
12 functionalizing the TiO_2 may alter the level alignment at the interface to reduce the injection loss
13 (capping moieties may offer the additional benefit of eliminating surface states that cause losses).
14
15
16
17
18
19
20
21
22
23
24
25
26
27
28

29 The crystalline environment is expected to enhance the screening and further reduce the gaps
30 of the dye-sensitized TiO_2 clusters. To estimate the magnitude of this effect we use an
31 electrostatic model for the polarization energy. P is the stabilization energy of an ionized
32 molecule due to screening by the surrounding molecules in a solid.⁵⁷⁻⁵⁸ The gap narrows by $2P$
33 because the ionization potential is decreased by P while the electron affinity is increased by P . P
34 is given in atomic units by:
35
36
37
38
39
40
41
42

$$P = -e^2 \frac{\epsilon - 1}{2R\epsilon} \quad (3)$$

43 where e is the electron charge, ϵ is the dielectric constant, and R is the effective volume per
44 molecule in the unit cell, given by:
45
46
47
48
49
50

$$R = \left(\frac{3V}{4\pi N} \right)^{1/3} \quad (4)$$

51 where V is the unit cell volume and N is the number of molecules in the cell. The dielectric
52 constant is obtained from the Clausius-Mossotti relation:
53
54
55
56
57
58
59
60

$$\frac{\varepsilon-1}{\varepsilon+2} = \frac{4\pi}{3V}\alpha \quad (5)$$

where α is the static polarizability. An accurate description of the polarizability, taking into account long-range screening effects, is provided within the many-body dispersion (MBD)⁵⁹ method by solving the Dyson-like self-consistent screening (SCS) equation from classical electrodynamics:

$$\alpha^{SCS}(\mathbf{r}; i\omega) = \alpha^{TS}(\mathbf{r}; i\omega) + \alpha^{TS}(\mathbf{r}; i\omega) \int d\mathbf{r}' T(\mathbf{r} - \mathbf{r}') \alpha^{SCS}(\mathbf{r}'; i\omega) \quad (6)$$

This equation relates the TS unscreened polarizability of an atom in a molecule,³¹ α^{TS} , to the fully screened polarizability, α^{SCS} , through the dipole-dipole interaction tensor, T . A detailed description of the method is provided in Refs. 59-60. This method has been shown to yield accurate dielectric constants for molecular crystals of polyacenes.⁶⁰ For pentacene, applying the polarization model to the $G_0W_0@CSP$ gas phase gap resulted in excellent agreement with periodic G_0W_0 calculations and experimental values for the fundamental gap of the crystal.

Table 2. Computed dielectric constants and polarization induced gap narrowing for the systems studied here.

System	ε	$2P$ (eV)
Ti ₂ cat ₂	3.72	1.78
Ti ₆ cat ₆	4.08	1.38

1
2
3 The computed dielectric constants and polarization induced gap narrowing of Ti_2cat_2 and
4 Ti_6cat_6 are given in Table 2. The estimated gaps of the crystalline Ti_2cat_2 and Ti_6cat_6 , obtained
5 from the polarization model, are shown in brown in Fig. 3. Applying the polarization model to
6 both systems results in identical gaps of 4.3 eV. This suggests that the screening in the crystalline
7 phase may mask the size effects in this case. We note that the model systems studied here are
8 smaller than the dyes and TiO_2 particles used in actual DSCs and consequently their gaps are
9 larger.

10
11 The optical gaps are expected to be smaller than the fundamental gaps computed here, owing
12 to the exciton binding energy. In addition, an injection mechanism involving a direct charge
13 transfer from the catechol HOMO to the conduction band of TiO_2 has been suggested.⁶¹⁻⁶⁸ These
14 phenomena, associated with neutral excitations, may be treated by solving the Bethe-Salpeter
15 equation on top of GW (GW/BSE), which is outside the scope of the present work. The accurate
16 description of the interface level alignment achieved here may provide the foundation for
17 subsequent treatment of optical excitations and injection dynamics.

18
19 To summarize, we employed recently developed dispersion-inclusive DFT and GW methods
20 to study the electronic structure of dye-sensitized TiO_2 clusters. We demonstrated that the
21 interface level alignment changes in an unintuitive way, owing to an intricate interplay of
22 quantum size effects and dynamic screening effects. The energy difference between the catechol
23 LUMO and the TiO_2 LUMO, which is associated with the injection loss in DSCs, may be
24 reduced significantly by reducing the dimensions of nano-structured TiO_2 and by functionalizing
25 the TiO_2 with wide-gap moieties, which contribute additional screening but do not interact
26 strongly with the frontier orbitals of the TiO_2 and the dye. We expect our conclusions regarding
27 the manifestation of size effects in the interface level alignment to be relevant to other hybrid
28
29
30
31
32
33
34
35
36
37
38
39
40
41
42
43
44
45
46
47
48
49
50
51
52
53
54
55
56
57
58
59
60

1
2
3 organic-inorganic functional nanostructures. We suggest that precise control of the electronic
4 structure may be achieved via “interface engineering” in such materials.
5
6
7
8
9

10 11 12 AUTHOR INFORMATION

13 14 **Corresponding Author**

15
16 *Email:nmarom@tulane.edu
17
18
19

20 21 **Author Contributions**

22
23 The manuscript was written through contributions of all authors. All authors have given approval
24 to the final version of the manuscript.
25
26
27

28 29 **Notes**

30
31 The authors declare no competing financial interest.
32
33
34
35
36

37 38 ACKNOWLEDGMENTS

39
40 Work at Tulane University was supported by the Louisiana Alliance for Simulation-Guided
41 Materials Applications (LA-SiGMA), funded by the National Science Foundation (NSF) award
42 number #EPS-1003897. Work at UT-Austin was supported by the Department of Energy for
43 work on nanostructures from grant DE-FG02-06ER46286. We also wish to acknowledge support
44 provided by the Scientific Discovery through Advanced Computing (SciDAC) program funded
45 by U.S. Department of Energy, Office of Science, Advanced Scientific Computing Research and
46 Basic Energy Sciences under award number DESC0008877 on algorithms. Computer time was
47 provided by the National Energy Research Scientific Computing Center (NERSC), which is
48
49
50
51
52
53
54
55
56
57
58
59
60

1
2
3 supported by the Office of Science of the U.S. Department of Energy under contract DE-AC02-
4 05CH11231.
5
6
7

8
9 **Supporting Information Available:** Crystal structure of $\text{Ti}_{17}\text{cat}_4$ with hydrogen positions,
10 including passivation of bridging oxygen sites; Detailed $\Delta v_{c,i}$ vs. $\Delta v_{x,i}$ plots used to find the
11 CSP for the systems studied here; Comparison of G_0W_0 @CSP spectra of catechol, calculated
12 with *tier 2* and *tier 4* basis sets, to gas phase photoemission spectroscopy. This material is
13 available free of charge via the Internet <http://pubs.acs.org>.
14
15
16
17
18
19
20
21
22
23
24
25
26
27
28
29
30
31
32
33
34
35
36
37
38
39
40
41
42
43
44
45
46
47
48
49
50
51
52
53
54
55
56
57
58
59
60

REFERENCES

- (1) Kroemer, H., *Nobel Lectures, Physics 1996-2000*. World Scientific Publishing Co.: Singapore, 2002.
- (2) Grätzel, M. Solar energy conversion by dye-sensitized photovoltaic cells. *Inorg. Chem.* **2005**, *44*, 6841-6851.
- (3) Grätzel, M. Recent Advances in Sensitized Mesoscopic Solar Cells. *Acc. Chem. Res.* **2009**, *42*, 1788-1798.
- (4) Hagfeldt, A.; Boschloo, G.; Sun, L. C.; Kloo, L.; Pettersson, H. Dye-Sensitized Solar Cells. *Chem. Rev.* **2010**, *110*, 6595-6663.
- (5) Grätzel, M.; Janssen, R. A. J.; Mitzi, D. B.; Sargent, E. H. Materials interface engineering for solution-processed photovoltaics. *Nature* **2012**, *488*, 304-312.
- (6) Umari, P.; Giacomazzi, L.; De Angelis, F.; Pastore, M.; Baroni, S. Energy-level alignment in organic dye-sensitized TiO₂ from GW calculations. *J. Chem. Phys.* **2013**, *139*, 014709.
- (7) Garcia-Lastra, J. M.; Rostgaard, C.; Rubio, A.; Thygesen, K. S. Polarization-Induced Renormalization of Molecular Levels at Metallic and Semiconducting Surfaces. *Phys. Rev. B* **2009**, *80*, 245427.
- (8) Garcia-Lastra, J. M.; Rostgaard, C.; Rubio, A.; Thygesen, K. S. Polarization-Induced Renormalization of Molecular Levels at Metallic and Semiconducting Surfaces (vol 80, 245427, 2009). *Phys. Rev. B* **2010**, *81*, 049901.
- (9) Garcia-Lastra, J. M.; Thygesen, K. S. Renormalization of Optical Excitations in Molecules Near a Metal Surface. *Phys. Rev. Lett.* **2011**, *106*, 187402.
- (10) Thygesen, K. S.; Rubio, A. Renormalization of Molecular Quasiparticle Levels at Metal-Molecule Interfaces: Trends Across Binding Regimes. *Phys. Rev. Lett.* **2009**, *102*, 046802.
- (11) Freysoldt, C.; Rinke, P.; Scheffler, M. Controlling Polarization at Insulating Surfaces: Quasiparticle Calculations for Molecules Adsorbed on Insulator Films. *Phys. Rev. Lett.* **2009**, *103*, 056803.
- (12) Neaton, J. B.; Hybertsen, M. S.; Louie, S. G. Renormalization of Molecular Electronic Levels at Metal-Molecule Interfaces. *Phys. Rev. Lett.* **2006**, *97*, 216405.

- 1
2
3
4
5
6
7
8
9
10
11
12
13
14
15
16
17
18
19
20
21
22
23
24
25
26
27
28
29
30
31
32
33
34
35
36
37
38
39
40
41
42
43
44
45
46
47
48
49
50
51
52
53
54
55
56
57
58
59
60
- (13) Migani, A.; Mowbray, D. J.; Iacomino, A.; Zhao, J.; Petek, H.; Rubio, A. Level Alignment of a Prototypical Photocatalytic System: Methanol on TiO₂(110). *J. Am. Chem. Soc.* **2013**, *135*, 11429-11432.
- (14) Migani, A.; Mowbray, D. J.; Zhao, J.; Petek, H.; Rubio, A. Quasiparticle Level Alignment for Photocatalytic Interfaces. *J. Chem. Theory Comput.* **2014**, *10*, 2103-2113.
- (15) Marom, N.; Kim, M.; Chelikowsky, J. R. Structure Selection Based on High Vertical Electron Affinity for TiO₂ Clusters. *Phys. Rev. Lett.* **2012**, *108*, 106801.
- (16) Chiodo, L.; Salazar, M.; Romero, A. H.; Laricchia, S.; Sala, F. D.; Rubio, A. Structure, Electronic, and Optical Properties Of TiO₂ Atomic Clusters: An Ab Initio Study. *J. Chem. Phys.* **2011**, *135*, 244704.
- (17) Mowbray, D. J.; Martinez, J. I.; Lastra, J. M. G.; Thygesen, K. S.; Jacobsen, K. W. Stability and Electronic Properties of TiO₂ Nanostructures With and Without B and N Doping. *J. Phys. Chem. C* **2009**, *113*, 12301-12308.
- (18) Hartmann Douma, D.; Gebauer, R. Optical Properties of Dye Sensitized TiO₂ Nanowires From Time-Dependent Density Functional Theory. *Phys. Status Solidi RRL* **2011**, *5*, 259-261.
- (19) Brennan, T. P.; Tanskanen, J. T.; Bakke, J. R.; Nguyen, W. H.; Nordlund, D.; Toney, M. F.; McGehee, M. D.; Sellinger, A.; Bent, S. F. Dynamical Orientation of Large Molecules on Oxide Surfaces and its Implications for Dye-Sensitized Solar Cells. *Chem. Mater.* **2013**, *25*, 4354-4363.
- (20) Sai, N.; Leung, K.; Chelikowsky, J. R. Hybrid Density Functional Study of Oligothiophene/ZnO Interface for Photovoltaics. *Phys. Rev. B* **2011**, *83*, 121309.
- (21) De Angelis, F.; Fantacci, S.; Selloni, A.; Nazeeruddin, M. K.; Grätzel, M. First-Principles Modeling of the Adsorption Geometry and Electronic Structure of Ru(II) Dyes on Extended TiO₂ Substrates for Dye-Sensitized Solar Cell Applications. *J. Phys. Chem. C* **2010**, *114*, 6054-6061.
- (22) De Angelis, F.; Fantacci, S.; Selloni, A.; Grätzel, M.; Nazeeruddin, M. K. Influence Of The Sensitizer Adsorption Mode on the Open-Circuit Potential of Dye-Sensitized Solar Cells. *Nano Lett.* **2007**, *7*, 3189-3195.
- (23) Nayak, P. K.; Garcia-Belmonte, G.; Kahn, A.; Bisquert, J.; Cahen, D. Photovoltaic Efficiency Limits and Material Disorder. *Energy Environ. Sci.* **2012**, *5*, 6022-6039.

- 1
2
3
4
5
6
7
8
9
10
11
12
13
14
15
16
17
18
19
20
21
22
23
24
25
26
27
28
29
30
31
32
33
34
35
36
37
38
39
40
41
42
43
44
45
46
47
48
49
50
51
52
53
54
55
56
57
58
59
60
- (24) Benedict, J. B.; Coppens, P. The Crystalline Nanocluster Phase as a Medium for Structural and Spectroscopic Studies of Light Absorption of Photosensitizer Dyes on Semiconductor Surfaces. *J. Am. Chem. Soc.* **2010**, *132*, 2938-2944.
- (25) Marom, N.; Moussa, J. E.; Ren, X. G.; Tkatchenko, A.; Chelikowsky, J. R. Electronic Structure of Dye-Sensitized TiO₂ Clusters from Many-Body Perturbation Theory. *Phys. Rev. B* **2011**, *84*, 245115.
- (26) Blum, V.; Gehrke, R.; Hanke, F.; Havu, P.; Havu, V.; Ren, X.; Reuter, K.; Scheffler, M. Ab Initio Molecular Simulations With Numeric Atom-Centered Orbitals. *Comput. Phys. Commun.* **2009**, *180*, 2175-2196.
- (27) Havu, V.; Blum, V.; Havu, P.; Scheffler, M. Efficient O(N) Integration for All-Electron Electronic Structure Calculation Using Numeric Basis Functions. *J. Comput. Phys.* **2009**, *228*, 8367-8379.
- (28) Ren, X.; Sanfilippo, A.; Rinke, P.; Wieferink, J.; Tkatchenko, A.; Reuter, K.; Blum, V.; Scheffler, M. An Accurate Resolution of Identity Approach to Hartree-Fock, Hybrid Functionals, MP2, RPA, And GW with Numeric Atom-Centered Basis Functions. *New J. Phys.* **2012**, *14*, 053020.
- (29) Perdew, J. P.; Burke, K.; Ernzerhof, M. Generalized Gradient Approximation Made Simple. *Phys. Rev. Lett.* **1996**, *77*, 3865-3868.
- (30) Perdew, J. P.; Burke, K.; Ernzerhof, M. Generalized Gradient Approximation Made Simple (vol 77, pg 3865, 1996). *Phys. Rev. Lett.* **1997**, *78*, 1396-1396.
- (31) Tkatchenko, A.; Scheffler, M. Accurate Molecular Van Der Waals Interactions from Ground-State Electron Density and Free-Atom Reference Data. *Phys. Rev. Lett.* **2009**, *102*, 073005.
- (32) Hedin, L. New Method For Calculating 1-Particle Green's Function with Application to the Electron-Gas Problem. *Phys. Rev.* **1965**, *139*, A796.
- (33) Hybertsen, M. S.; Louie, S. G. Electron Correlation in Semiconductors and Insulators - Band-Gaps and Quasi-Particle Energies. *Phys. Rev. B* **1986**, *34*, 5390-5413.
- (34) Onida, G.; Reining, L.; Rubio, A. Electronic Excitations: Density-Functional Versus Many-Body Green's-Function Approaches. *Rev. Mod. Phys.* **2002**, *74*, 601-659.

- 1
2
3
4 (35) Marom, N.; Caruso, F.; Ren, X.; Hofmann, O. T.; Körzdörfer, T.; Chelikowsky, J. R.;
5 Rubio, A.; Scheffler, M.; Rinke, P. Benchmark of GW Methods for Azabenzenes. *Phys. Rev. B*
6 **2012**, *86*, 245127.
7
8 (36) Jiang, H.; Gomez-Abal, R. I.; Rinke, P.; Scheffler, M. First-Principles Modeling of
9 Localized d States with the GW@LDA+U Approach. *Phys. Rev. B* **2010**, *82*, 045108.
10
11 (37) Qteish, A.; Rinke, P.; Scheffler, M.; Neugebauer, J. Exact-Exchange-Based Quasiparticle
12 Energy Calculations for the Band Gap, Effective Masses, and Deformation Potentials Of ScN.
13 *Phys. Rev. B* **2006**, *74*, 245208
14
15 (38) Rinke, P.; Qteish, A.; Neugebauer, J.; Freysoldt, C.; Scheffler, M. Combining GW
16 Calculations with Exact-Exchange Density-Functional Theory: An Analysis of Valence-Band
17 Photoemission for Compound Semiconductors. *New J. Phys.* **2005**, *7*, 126
18
19 (39) Rinke, P.; Qteish, A.; Neugebauer, J.; Scheffler, M. Exciting Prospects for Solids: Exact-
20 Exchange Based Functionals Meet Quasiparticle Energy Calculations. *Phys. Status Solidi B*
21 **2008**, *245*, 929-945.
22
23 (40) Rinke, P.; Scheffler, M.; Qteish, A.; Winkelkemper, M.; Bimberg, D.; Neugebauer, J.
24 Band Gap and Band Parameters Of InN and GaN from Quasiparticle Energy Calculations Based
25 on Exact-Exchange Density-Functional Theory. *Appl. Phys. Lett.* **2006**, *89*, 161919
26
27 (41) Fuchs, F.; Bechstedt, F. Indium-Oxide Polymorphs from First Principles: Quasiparticle
28 Electronic States. *Phys. Rev. B* **2008**, *77*, 155107.
29
30 (42) Rodl, C.; Fuchs, F.; Furthmüller, J.; Bechstedt, F. Quasiparticle Band Structures of the
31 Antiferromagnetic Transition-Metal Oxides MnO, FeO, CoO, and NiO. *Phys. Rev. B* **2009**, *79*,
32 235114.
33
34 (43) Perdew, J. P.; Zunger, A. Self-Interaction Correction to Density-Functional
35 Approximations for Many-Electron Systems. *Phys. Rev. B* **1981**, *23*, 5048-5079.
36
37 (44) Körzdörfer, T.; Kümmel, S.; Marom, N.; Kronik, L. When to Trust Photoelectron Spectra
38 from Kohn-Sham Eigenvalues: The Case of Organic Semiconductors. *Phys. Rev. B* **2009**, *79*,
39 201205.
40
41 (45) Körzdörfer, T.; Kümmel, S.; Marom, N.; Kronik, L. When to Trust Photoelectron Spectra
42 from Kohn-Sham Eigenvalues: The Case of Organic Semiconductors (vol 79, 201205, 2009).
43 *Phys. Rev. B* **2010**, *82*, 129903.
44
45
46
47
48
49
50
51
52
53
54
55
56
57
58
59
60

- 1
2
3
4
5
6
7
8
9
10
11
12
13
14
15
16
17
18
19
20
21
22
23
24
25
26
27
28
29
30
31
32
33
34
35
36
37
38
39
40
41
42
43
44
45
46
47
48
49
50
51
52
53
54
55
56
57
58
59
60
- (46) Körzdörfer, T. On the Relation Between Orbital-Localization and Self-Interaction Errors in the Density Functional Theory Treatment of Organic Semiconductors. *J. Chem. Phys.* **2011**, *134*, 094111.
- (47) Marom, N.; Ren, X. G.; Moussa, J. E.; Chelikowsky, J. R.; Kronik, L. Electronic Structure of Copper Phthalocyanine from G_0W_0 Calculations. *Phys. Rev. B* **2011**, *84*, 195143.
- (48) Salomon, E.; Amsalem, P.; Marom, N.; Vondracek, M.; Kronik, L.; Koch, N.; Angot, T. Electronic Structure of CoPc Adsorbed on Ag(100): Evidence for Molecule-Substrate Interaction Mediated by Co 3d Orbitals. *Phys. Rev. B* **2013**, *87*, 075407.
- (49) Atalla, V.; Yoon, M.; Caruso, F.; Rinke, P.; Scheffler, M. Hybrid Density Functional Theory Meets Quasiparticle Calculations: A Consistent Electronic Structure Approach. *Phys. Rev. B* **2013**, *88*, 165122.
- (50) Körzdörfer, T.; Marom, N. A Strategy for Finding a Reliable Starting Point for G_0W_0 Demonstrated for Molecules. *Phys. Rev. B* **2012**, *86*, 041110(R)
- (51) The comparison between different systems, calculated based on functionals with different fractions of exact exchange, is an inherent feature of any electronic structure method containing system dependent parameters [e.g., Ref 49; Karolewski, A., Kronik, L.; Kümmel, S. Using Optimally Tuned Range Separated Hybrid Functionals in Ground-State Calculations: Consequences and Caveats *J. Chem. Phys.* **2013**, *138*, 204115; Himmetoglu, B., Floris, A., de Gironcoli, S.; Cococcioni, M. Hubbard-corrected DFT Energy Functionals: The LDA+U Description of Correlated Systems *Int. J. Quantum Chem.* **2014**, *114*, 14; Dabo I., Ferretti A., Poilvert N., Li Y. L., Marzari N., Cococcioni M. Koopmans' Condition for Density-Functional Theory *Phys. Rev. B* **2010**, *82*, 115121]. Such comparisons are justified under the assumption that the system dependent parameters reflect a physical property of the system. In this case, the amount of EXX in the CSP is inversely related to the extent of screening.
- (52) Chiodo, L.; Garcia-Lastra, J. M.; Iacomino, A.; Ossicini, S.; Zhao, J.; Petek, H.; Rubio, A. Self-Energy and Excitonic Effects in the Electronic and Optical Properties of TiO_2 Crystalline Phases. *Phys. Rev. B* **2010**, *82*, 045207.
- (53) Kang, W.; Hybertsen, M. S. Quasiparticle and Optical Properties of Rutile and Anatase TiO_2 *Physical Review B* **2010**, *82*, 085203.
- (54) van Schilfgaarde, M.; Kotani, T.; Faleev, S. Quasiparticle Self-Consistent GW Theory. *Phys. Rev. Lett.* **2006**, *96*, 226402.

1
2
3
4
5
6
7
8
9
10
11
12
13
14
15
16
17
18
19
20
21
22
23
24
25
26
27
28
29
30
31
32
33
34
35
36
37
38
39
40
41
42
43
44
45
46
47
48
49
50
51
52
53
54
55
56
57
58
59
60

(55) Thulin, L.; Guerra, J. Calculations of Strain-Modified Anatase TiO₂ Band Structures. *Phys. Rev. B* **2008**, *77*, 195112.

(56) We note that the GW gaps reported here are larger than the gaps obtained in Ref. 24 using a hybrid DFT functional. Hybrid functionals do not generally provide accurate gaps [see: Jain, M.; Chelikowsky, J. R.; Louie, S. G. Reliability of Hybrid Functionals in Predicting Band Gaps *Phys. Rev. Lett.* **2011**, *107*, 216806]. In some cases the underestimated gaps obtained with hybrid DFT functionals may fortuitously agree with measured optical gaps.

(57) Sato, N.; Seki, K.; Inokuchi, H. Ultraviolet Photoelectron Spectra of Tetrahalogeno-p-benzoquinones and Hexahalogenobenzenes in the Solid State. *J. Chem. Soc., Faraday Trans. 2* **1981**, *77*, 47-53.

(58) Hill, I. G.; Kahn, A.; Soos, Z. G.; Pascal, J. R. A. Charge-Separation Energy in Films of π -Conjugated Organic Molecules. *Chem. Phys. Lett.* **2000**, *327*, 181-188.

(59) Tkatchenko, A.; DiStasio, R. A., Jr.; Car, R.; Scheffler, M. Accurate and Efficient Method for Many-Body van der Waals Interactions. *Phys. Rev. Lett.* **2012**, *108*, 236402.

(60) Schatschneider, B.; Liang, J.-J.; Reilly, A. M.; Marom, N.; Zhang, G.-X.; Tkatchenko, A. Electrodynamic Response and Stability of Molecular Crystals. *Phys. Rev. B* **2013**, *87*, 060104.

(61) Duncan, W. R.; Prezhdo, O. V. Electronic Structure and Spectra of Catechol and Alizarin in the Gas Phase and Attached to Titanium. *J. Phys. Chem. B* **2005**, *109*, 365-373.

(62) Duncan, W. R.; Prezhdo, O. V. Theoretical Studies of Photoinduced Electron Transfer in Dye-Sensitized TiO₂. *Annu. Rev. Phys. Chem.* **2007**, *58*, 143-184.

(63) Gundlach, L.; Ernstorfer, R.; Willig, F. Ultrafast Interfacial Electron Transfer from the Excited State of Anchored Molecules into a Semiconductor. *Prog. Surf. Science* **2007**, *82*, 355-377.

(64) Prezhdo, O. V.; Duncan, W. R.; Prezhdo, V. V. Photoinduced Electron Dynamics at the Chromophore-Semiconductor Interface: A Time-Domain Ab Initio Perspective. *Prog. Surf. Science* **2009**, *84*, 30-68.

(65) Redfern, P. C.; Zapol, P.; Curtiss, L. A.; Rajh, T.; Thurnauer, M. C. Computational Studies of Catechol and Water Interactions with Titanium Oxide Nanoparticles. *J. Phys. Chem. B* **2003**, *107*, 11419-11427.

(66) Lundqvist, M. J.; Nilsing, M.; Persson, P.; Lunell, S. DFT Study of Bare and Dye-Sensitized TiO₂ Clusters and Nanocrystals. *Int. J. Quantum Chem.* **2006**, *106*, 3214-3234.

1
2
3 (67) Persson, P.; Bergström, R.; Lunell, S. Quantum Chemical Study of Photoinjection
4 Processes in Dye-Sensitized TiO₂ Nanoparticles. *J. Phys. Chem. B* **2000**, *104*, 10348-10351.
5

6
7 (68) Snoeberger, R. C.; Young, K. J.; Tang, J.; Allen, L. J.; Crabtree, R. H.; Brudvig, G. W.;
8 Coppins, P.; Batista, V. S.; Benedict, J. B. Interfacial Electron Transfer into Functionalized
9 Crystalline Polyoxotitanate Nanoclusters. *J. Am. Chem. Soc.* **2012**, *134*, 8911-8917.
10
11
12
13
14
15
16
17
18
19
20
21
22
23
24
25
26
27
28
29
30
31
32
33
34
35
36
37
38
39
40
41
42
43
44
45
46
47
48
49
50
51
52
53
54
55
56
57
58
59
60

